Nuclear Engineering and Design 424 (2024) 113260

Contents lists available at ScienceDirect

Nuclear Engineering and Design

journal homepage: www.elsevier.com/locate/nucengdes

Numerical and analytical investigation of thermal hydraulic behavior of large pools in passive heat exchangers

Tahmineh Adili *, Iurii Dolganov, Filip Janasz, Stephan Leyer

Department of Engineering, Faculty of Science, Technology and Medicine, University of Luxembourg, L-1359 Luxembourg, Luxembourg

ARTICLE INFO

Keywords:
Nucleate pool boiling
Two-phase flow
CFD simulation
Passive Heat Removal Systems (PHRS)

ABSTRACT

Passive residual heat removal safety systems are a modern design concept employed in Nuclear Power Plants (NPPs), and operate based on natural circulation. Several passive safety systems such as the emergency condensers (EC) use heat exchanger tube bundles immersed in large pools of coolant acting as a heat-sink (secondary side). The primary side of the heat exchanger is connected to the reactor core and, when activated, removes the decay heat in case of an accident. Recent research revealed the limitation of the state-of-the-art heat transfer models to capture the heat transfer rates achieved in these systems. The problems can be identified in both – primary and the secondary sides. The main focus of this study is to investigate the thermal hydraulic behavior of the secondary side of an EC. The data from the NOKO test facility has been considered as the validation base of this study. It has been observed that strong temperature stratification establishes in the pool due to the heat transfer process happening in a confined volume zone. Under this condition, the saturation temperature is reached at higher elevations of the tank while lower the liquid remains subcooled. This leads to different thermal behavior of the liquid at different elevations in the tank which is not properly captured by simple models. In addition, due to the complexity of the heat transfer process the required computational power is another challenge to study the thermal hydraulic behavior of the system. Therefore, the main aim of this study was to correctly predict the temperature stratification in the pool and identify boiling onset at different locations specially on the heated surfaces, while maintaining minimum numerical complexity. To achieve these targets, 2D multi-phase CFD simulations of secondary side using two different frameworks was conducted using ANSYS Fluent. Then, the results were validated against experimental data to assess their accuracy to achieve the best simulation approach.

1. Introduction

Passive heat removal systems (PHRS) play a major role in ensuring safety of the nuclear power plants even in a case of complete station blackout. These systems operate based on natural convection, which increases their reliability. One notable reactor design that incorporates various PHRS components is the KERENA reactor concept (formerly SWR1000), a Generation III + design. The KERENA reactor integrates essential PHRS elements such as containment cooling condensers (CCC), emergency condensers (EC), and passive core flooding systems. This work focuses on the performance of emergency condensers (EC) during potential accidents in the KERENA reactor.

An EC is designed as a safety measure to handle the transfer of decay heat from the core to the coolant in large pools. The system includes a heat exchanger composed of bundles of slightly inclined U-shaped tubes submerged in water (see Fig. 1). In the event of an accident, as the water level in the reactor pressure vessel decreases, the EC U-tubes (primary side) gradually fill with steam. Steam inside the tubes condenses upon thermal contact with the cold water in the pool (secondary side) via tubes' walls. Condensed water then flows back to the reactor's pressure vessel. This process is driven by the density difference and gravitational force.

Numerous studies have been devoted to exploring the thermal hydraulic characteristics and assess the heat dissipation potential of ECs. This focus stems from the need to accurately predict heat transfer capabilities with the aim of potential design optimization (Cooper, 1984; Gorenflo, 1993; Chun and Kang, 1998) and accurate understanding of the system performance to provide correct information for NPP accident analysis and safety assessments. Notable advancements have been achieved in the analysis and prediction of condensation process of

* Corresponding author.
E-mail address: Tahmineh.adili@uni.lu (T. Adili).

https://doi.org/10.1016/j.nucengdes.2024.113260
Received 18 January 2024; Received in revised form 7 April 2024; Accepted 27 April 2024
Available online 1 May 2024

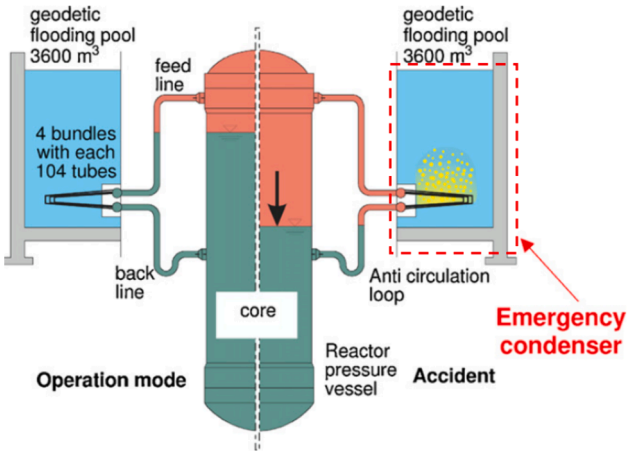

Fig. 1. Operation Principle of an Emergency Condenser (Krepper and Beyer, 2010).

superheated steam in the primary side of ECs (Zhang, 2019; Shabestary, 2020); nevertheless, there remains room for further progress to attain a comparable level of comprehension of the processes occurring on the secondary side of these heat exchangers. On the secondary side, natural convection in a large pool with unstirred fluids, leads to the formation of temperature stratification which increases the difficulty of correct prediction of EC performance. During EC operation, the heat transfer in secondary side starts with single phase natural convection and then shifts to subcooled and nucleate pool boiling as the coolant heats up. The generation of steam in the pool has an impact on the fluid velocity and disrupts the established temperature stratification. Additionally, steam produced in the pool has the potential to escape into the containment atmosphere, thereby increasing the pressure inside a containment. This pronounced temperature stratification results in the attainment of the saturation condition at the uppermost region of a pool at an accelerated pace, in contrast to a condition where the temperature profile is uniformly distributed. Consequently, this triggers an early initiation of the boiling process in a pool due to elevated localized temperatures manifesting in the upper regions (Stephan and Abdelsalam, 1980). This results in an earlier pressure buildup on the containment compared to calculations based on the assumption of a uniform temperature in the pool. On the other hand, the lower temperatures below the stratification layer may improve the heat transfer conditions within the tubes bundle temporarily. These all leads to significant challenges to accurately predict the thermal hydraulic behavior of the system during the operation. Therefore, the primary objective of this study is to attain an accurate prediction of the temperature profile in the pool and cooling capacity of the heat exchanger during the operation of an EC. This offers essential insights into the factors influencing temperature stratification in the pool, enhancing our understanding of the system's ability to dissipate decay heat during accidents.

Existing literature offers a multitude of empirical or semi-empirical correlations, which have been suggested to estimate the heat transfer coefficient for external flows around an individual tube or a bundle of tubes within various types of heat exchangers, incorporating natural convection and nucleate pool boiling mechanisms (Cooper, 1984; Gorenflo, 1993; Chun and Kang, 1998; Stephan and Abdelsalam, 1980; Rohsenow, 1952; Forster and Zuber, 1955; Cornwell and Houston, 1994; Kutateladze and Borishanskii, 2021; Kruzhilin, 1947; Labuntsov, 1973). Previous investigations have focused on the examination of heat transfer performance in heat exchangers, considering various factors that influence the heat transfer process and the determination of the heat transfer coefficient. Nonetheless, due to the limited application range of these studies and the intricate nature of the pool boiling mechanism in large size heat exchangers, their ability to accurately predict the heat transfer performance of an EC remains inadequate. In addition, to demonstrate the physical behavior of the fluid in this process, some numerical studies have been conducted to explore the phenomena of natural convection and pool boiling in large, confined spaces in ECs (Tian et al., 2017). The most relevant study is from Krepper et al. (2007) who conducted a numerical analysis of natural circulation and temperature stratification in large pools in a two-dimensional (2D) setting. They focused on the application of an EC, specifically studying large volume pools heated by a bundle of U-shaped tubes submerged in a water tank based on NOKO test facility experiments. The objective of their work was to predict temperature distribution and stratification of the fluid in the secondary side of this test apparatus. Using experimental data, they showed that in NOKO test facility the contribution of the U-bend region of heated tubes compared to total heat flux transferred to the cooling water in the secondary side is negligible (Krepper and Beyer, 2010; Krepper et al., 2000). Therefore, 2D CFD modeling seems like a feasible approach. However, the scale of simplifications they used in their calculations, led to considerable discrepancy of calculations from experimental data. For instance, they employed a constant heat flux as boundary condition only in the upper bundle and considered a moment in accident progression when lower part of the bundle is still filled with cold water. In contrast, this study adopts more precise boundary conditions derived from the inherent characteristics of the heat-up process and corroborated by experimental data. Furthermore, because of high computational efforts they needed for their calculations, their work suffers from a lack of comprehensive evaluation based on the experimental data of NOKO facility. Hence, enhancing the accuracy and practically of these simulations have been considered as the main target in this study. In this study, the objective is to maintain calculations within an economically viable range while enhancing the precision of calculations to predict the thermal–hydraulic behavior of the fluid on the secondary side.

In another word, in this work, it is aimed to enhance the understanding of heat transfer performance in a specific type of heat exchanger, particularly in subcooled and nucleate boiling regions. To achieve this goal, a systematic approach was adopted, beginning with 2D CFD simulations employing various methods. The aim was to identify the most suitable modeling framework for our application by comparing the simulation results with experimental data. The research focused on the NOKO-HZDR test facility as a validation base, leveraging its high-quality data and configuration similarity to real-scale EC systems (Krepper and Beyer, 2010; Hicken et al., 2000). However, due to experimental constraints limiting the investigation of natural circulation in NOKO test rig, particularly the velocity distribution in this region, simulations became essential. These simulations are used to demonstrate the coolant's temperature and velocity distribution in the secondary side, providing insights challenging to obtain through experiments. To address computational costs, the study employed 2D multi-phase CFD simulations using ANSYS Fluent. The evaluation of results centered on two multi-phase approaches: the mixture model and the inhomogeneous Eulerian model. The mixture model was chosen for its ability to simplify the modeling of phase change in subcooled boiling regions and reduce computational costs. However, recognizing the complexity of the process, the inhomogeneous Eulerian model was also incorporated, employing empirical models to capture evaporation and condensation phenomena, thereby enhancing simulation accuracy. There are different advantages using this methodology compared to previous works. Firstly, the research is initiated by subjecting more simplified methods to examination, evaluating their capability to accurately model the thermal–hydraulic behavior of the fluid in the process. This facilitates the identification of a cost-effective approach for understanding the phenomenon. Secondly, more accurate boundary conditions are employed, contributing to a reduction in simulation disparities without necessitating an increase in the complexity of the simulation models. Consequently, a manageable and realistic range of computations is maintained. All simulation results were meticulously validated against experimental data from NOKO-HZDR. Additionally, a heat balance analysis was conducted, aligning with experimental data to

conclude the study. Overall, the research aimed to contribute to develop insights into heat transfer phenomena and thermal hydraulic behavior in EC systems, offering a comprehensive understanding achieved through a structured methodology and rigorous validation against experimental data.

2. NOKO-HZDR test facility

The NOKO test facility has been launched in Forschungszentrum Jülich (FZJ) to assess the thermal hydraulic efficiency of the passive decay heat removal systems in different pressure (up to 7 MPa) and power (4 MW) operating conditions (Hicken and Verfondern, 2000). In 2005, the test facility was relocated to Forschungszentrum Rossendorf (HZDR), where experiments were conducted to perform a detailed analysis of the two-phase flow on the secondary side. The NOKO-HZDR has been installed in the TOPFLOW (Transient TwO-Phase FLOW) test facility with the improved instrumentation concept to measure the temperature field on the secondary side with higher resolution. The NOKO-HZDR component was constructed using the same materials and dimensions as an emergency condenser found in a SWR1000 reactor, with the only modification being a reduction in the number of tubes in the bundles. The NOKO facility comprises horizontally oriented U-shaped tubes with a length of approximately 10,000 mm, an inner diameter of 44.5 mm, and a tube wall thickness of 2.9 mm. These tubes are arranged in bundles and are submerged in a cooling water medium contained within a horizontally cylindrical tank. The tank has a length of 6 m, an inner diameter of 2 m, and a total volume of 20 m^3 (see Fig. 2-a) (Hicken and Verfondern, 2000). The bundles of tubes are submerged in the cooling water located in the tank.

The improved instrumentation of the NOKO secondary side in the FZR consists of 11 × 8 type K thermocouples installed in the tank to record temperature changes in the heat up process. Eleven thermocouples are placed at each of the eight cross-sectional planes (A-H) along the tubes (see Fig. 2-a) in different locations (see Fig. 2-b). The commencement of the heat transfer process occurs in response to an accident within the reactor. During this event, steam replaces water in the upper bundle of the U-tubes. Notably, at this initial stage, the lower portion of the bundle remains filled with cold water, setting the foundation for subsequent thermal dynamics and providing valuable insights into the behavior of the system.

NOKO experiments have been carried out under four different working conditions which are regulated based on the pressure of the primary side. Table 1, shows the experiment conditions of NOKO-HZDR.

In NOKO experiments the secondary side is heated from approx. 20 ℃–32 ℃ to the saturation temperature while the pressure in the tank is maintained close to ambient pressure. The pressure within the primary side, as well as within the inlet and outlet collectors, undergoes a decrease along with the temperature gradient from the inlet to the outlet, transitioning from superheated steam conditions to the saturation state as liquid water exits the system. The high heat flux from primary side to the secondary side leads to a non-uniform temperature profile in the tank. Strong thermal stratification and temporal temperature jumps (sudden temperature increase) at different levels of the cooling water in the tank have been demonstrated during the experiments in the NOKO facility (see “Big” and “Small Jumps” in Fig. 3). Based on the transient temperature measurements data, it can be observed that the temperature distribution along the length of tube bundles is nearly uniform (Krepper and Beyer, 2010). Fig. 3 shows the temperatures transient recorded with 11 thermocouples located in one measuring plane (plane D) when the operating pressure of the primary side is equal to 65 bar (Kutateladze and Borishanskii, 2021).

3. Numerical simulations

3.1. 2D CFD simulations

Two multiphase models have been used to calculate the temperature stratification in secondary side of an EC. The first was a mixture model combined with a semi-mechanistic boiling model to simulate interphase mass transfer.

Mixture model is suitable for subcooled boiling, treating vapor and liquid phases as interpenetrating continua governed by a common set of equations (see chapter 14 in (ANSYS, 2022). The model assumes that the phases are in a state of local thermodynamic equilibrium and computes interfacial transfer terms by employing empirical closure relationships. This relationship leverages a transport equation to model the interfacial area concentration, accounting for coalescence resulting from random collisions driven by turbulence, as well as breakage due to the impact of turbulence eddies. These phenomena are informed by the seminal contributions of Hibiki and Ishii (2000). For more details of the equations used for this model see chapter 14.4 in (ANSYS, 2022). The second used multiphase model uses an inhomogeneous Eulerian approach, which is well-regarded for its precision in predicting the thermal behavior of bubbly flows, especially when they are close to saturation condition (Lawrence, 2020). In this model, each phase is treated separately with its own set of properties and transport equations (Lawrence, 2020).

In mixture model approach, Schiller-Naumann model is used to calculate the drag force coefficient and a standard k-ε model with enhanced wall treatment as turbulence model. In addition, a semi-mechanistic boiling model has been added to this simulation. It is an empirical model to calculate the boiling on the heated walls developed by Hibiki and Ishii 2000). It calculates the nucleate boiling heat transfer c(oefficient using Foster and Zuber correlation (Hibiki and Ishii, 2000). To calculate the slip velocity the Manninet-et-al model has been employed. A continuum surface tension force modelling for water and vapor phases is added to the simulation setup (Hicken, et al., 2000).

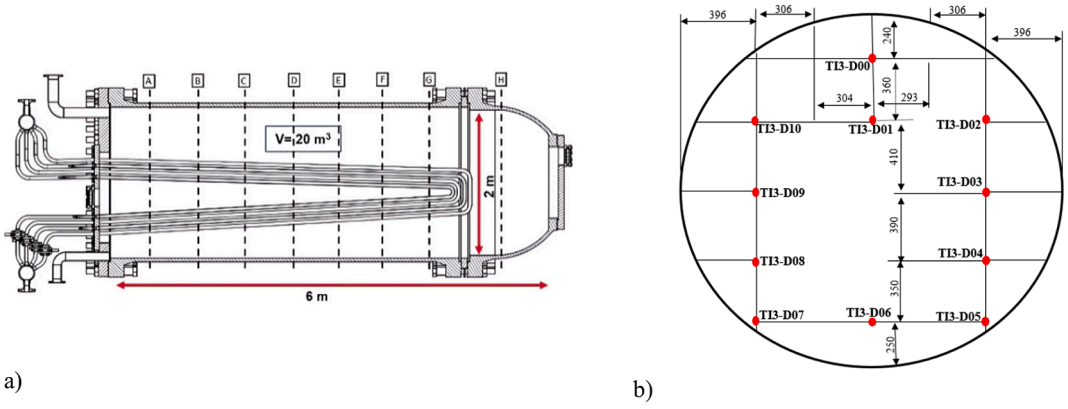

Fig. 2. The Geometry of the NOKO_EC with measuring planes and location of thermocouples (Krepper and Beyer, 2010; Hicken and Verfondern, 2000).

Table 1
Experimental conditions for NOKO-HZDR (Hollands et al., 2016).

Experiment No.	Primary side Pressure [MPa]	Secondary side pressure [MPa]	Mass flow rate of primary side [kg/s]	Differential pressure at end of collectors [MPa]	Initial temperature of Secondary side [°C]	Level of water in tank [m]	Power of the HX at steady state [MW]
10 bar	0.994–1.072	0.137–0.156	0–0.065	0–0.02	Approx. 32.5	1.688–1.743	1.35
30 bar	3.024–3.070	0.133–0.182	0–1.47	0–0.02	Approx. 20.0	1.688–1.792	2.545
50 bar	5.076–5.090	0.133–0.186	0–1.70	0–0.05	Approx. 22.0	1.673–1.717	3.117
65 bar	6.476–6.820	0.133–0.155	0–2.52	0–0.05	Approx. 25.5	1.653–1.719	4.011

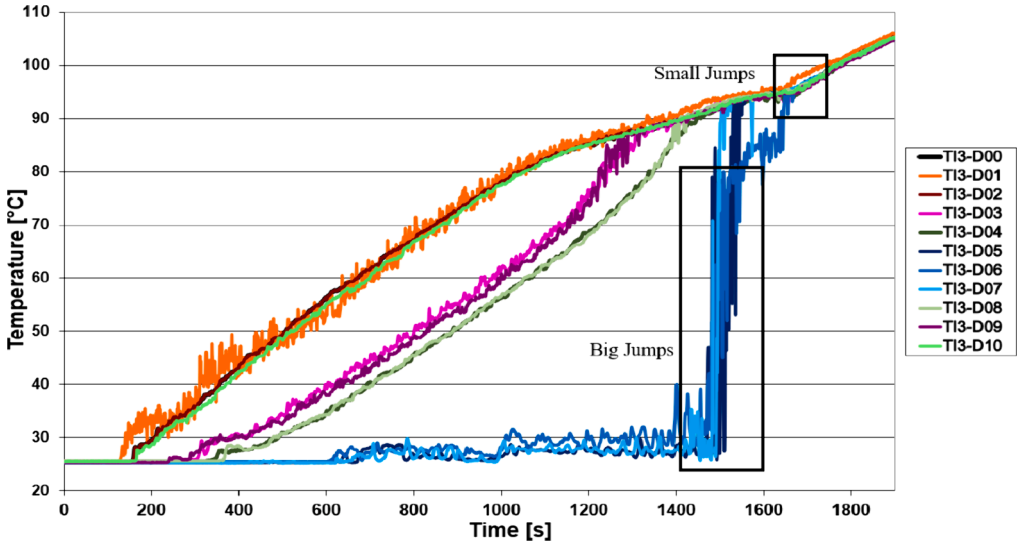

Fig. 3. Experimental transient temperature distribution of the secondary side on plane D at 65 bar operating condition in primary side (Krepper and Beyer, 2010).

The Inhomogeneous Eulerian model uses Schiller and Naumann model (Schiller, 1933) to calculate drag force and Tomiyama (1992) model is used to calculate lift force. Turbulent dispersion and turbulence interaction have been taken into account by using Tomiyama (1992) model and Sato and Sekoguchi, 1979 respectively. In Eulerian model, thermal phase change model becomes applicable in instances of evaporation condensation alongside the two-resistance approach to calculate phase heat transfer coefficients. This is useful in Eulerian framework, since the mass transfer process of evaporation- condensatin is exclusively regulated by interphase heat transfer mechanisms and the overall heat balance. Therefore, no calibration is required for mass transfer coefficients and it makes the use of two-resistance heat transfer method more feasible (Chapter 14 Ref (ANSYS, 2022)). Two-resistance heat transfer model is suitable to consider the interphase heat transfer process accurately. In this approach, distinct computations are conducted to determine heat transfer coefficients independently on each side of the phase interface (see Chapter 14 in (ANSYS, 2022). In this calculation, Ranz-Marshall model is used to calculate heat transfer for liquid side and zero-resistance model is used for the vapor side of the fluid. To calculate the turbulence effects in the simulation, a standard k-ε model with enhanced wall treatment has been used.

The position of the measuring plane D (see Fig. 2) has been chosen for 2D CFD simulation as it is located in the middle of the tube bundle in the tank. In both simulations, an unstructured mesh was utilized with varying volumes to ensure accurate representation of flow phenomena near and away from solid boundaries. Specifically, a minimum volume of $2.31 \times 10^{-6} m^3$ was allocated to regions adjacent to the walls, while regions farther away were assigned a volume of $1.53 \times 10^{-3} m^3$. This mesh configuration facilitates the capture of boundary layer effects near surfaces while maintaining computational efficiency in regions with lower flow gradients. The boundary conditions of these simulations have been set to match the NOKO facility operational conditions. The detailed boundary and initial condition of 2D simulation set up are shown in Fig. 4. For these simulations, we incorporated a constant temperature boundary condition (210 °C) for the upper bundle and a time-dependent temperature boundary condition for the lower bundle as shown in Fig. 6. This decision is based on the trend observed in the experimental data, Fig. 5, where the fluid outlet temperature within the bundles initiates a gradual increase approximately 200 s after the commencement of the process. This increase continues until a steady-state condition is achieved at a constant temperature after 1100 s. Given that, the simulation focuses on the central location within the tank and taking into account the calculated fluid mass flow rate in the tubes, the time required for the temperature of the lower bundle to initiate an increase and subsequently reach a stable state had been determined. Meanwhile, the temperature profile shown in Fig. 5, corresponds to the fluid inside the tubes. Therefore, the outer wall temperature can be determined using correlations for the conduction heat transfer mechanism. To calculate the value of the transient boundary condition, Eq. (1) is used. In this equation, λ is thermal conductivity of the tube's wall, and dx is tubes thickness.

The wall of the tank has been considered as adiabatic wall and the free surface boundary condition is used at the top of the cooling water, ensuring free-slip. The initial operating pressure is 0.1 MPa (ambient pressure), since the blow-off valves of the secondary side tank is open for the experiment and floating operating pressure is applied in the simulation. The initial temperature for liquid in the secondary side is 300 K.

3.2. Numerical simulations results

2D simulation with mixture model

Temperature distribution and fluid velocity in the pool for 65 bars in the primary side case are shown in sequence of figures presented in Fig. 7 at different simulation times. These figures provide a visual

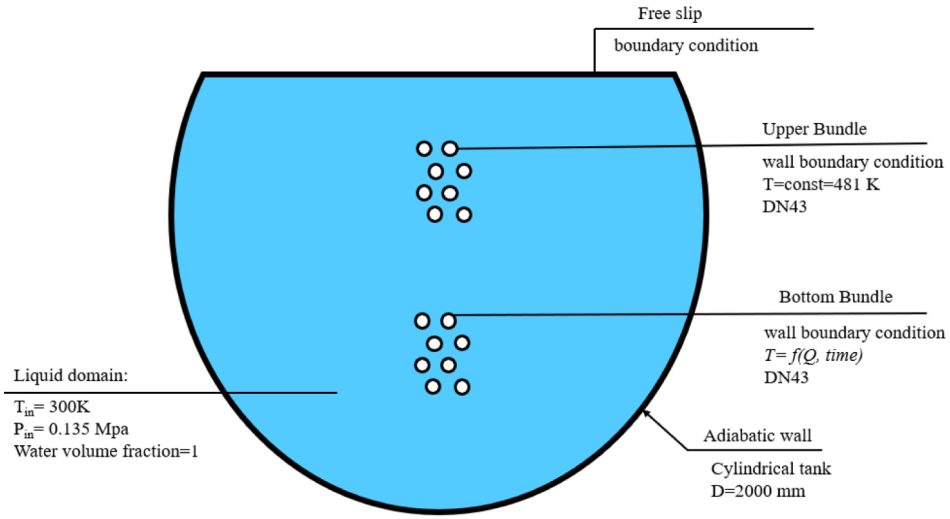

Fig. 4. Initial and Boundary Condition of 2D CFD Simulation.

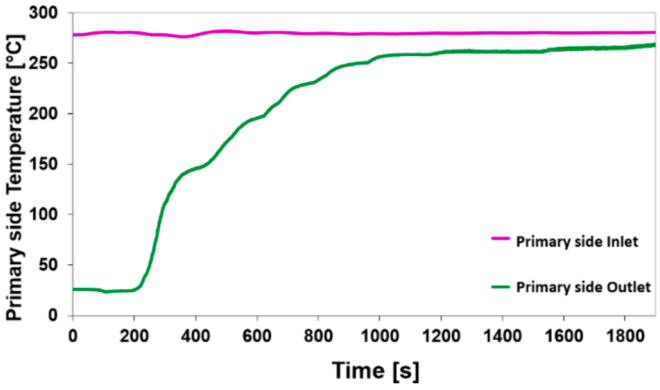

Fig. 5. Measured temperature of inlet and outlet of the primary side.

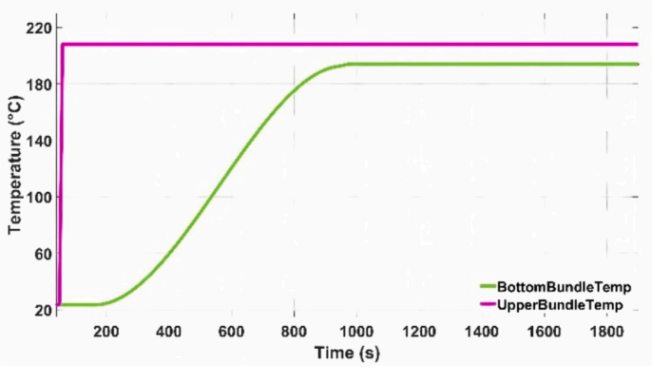

Fig. 6. Temperature boundary condition used in calculation

representation of how the temperature distribution and velocity contours evolve over simulation time, offering valuable insights into the dynamic nature of natural circulation systems. The figures related to the temperature distributions, highlight the temperature stratification in the secondary side, whereas a stagnant zone forms at the bottom of the tank. This stagnant zone initially maintains a relatively constant temperature until the upper regions of the tank approach saturation temperature. During this phase, heat transfer primarily occurs through natural convection, leading to a gradual warming of the stagnant zone.

As the heat-up process progresses, the stagnant zone gradually dissipates as the temperature differential between the bottom and upper regions diminishes. However, even after 1800 s from the beginning of the process, this zone persists to some extent. While saturation temperatures are observed in the upper regions of the tank at this time according to experimental data, such a change is not fully reflected in the calculations. This transition is marked by a sudden temperature increase in the lower part of the tank, as evidenced by experimental data at approximately t ≈ 1500 s (see Fig. 3).

The velocity contours provide a visual representation of the flow pattern established during natural circulation. In regions characterized by higher fluid velocity (around the higher bundle), such as those experiencing increased convection, temperature gradients diminish more rapidly due to enhanced heat transfer. Consequently, these regions undergo faster temperature increases compared to areas with lower fluid velocity.

At the onset of the heat-up process, the calculations conducted via the mixture model reveal a relatively uniform velocity distribution. Regions with higher velocities predominantly align with the upper sections of the tank, nearer to the water surface, and are subject to elevated heat flux due to the higher temperatures of tube boundary conditions. However, areas proximate to the lower tubes bundle in the tank exhibit significantly lower velocities (approximately 0.0342 m/s2) and display smaller vortices, resulting in a subdued temperature increase in this vicinity.

The computations have been carried out using an unstructured mesh with 114,254 elements and the computational tasks were executed on a High-Performance Computing (HPC) cluster, utilizing a single node comprising 128 processing cores. The simulations encompassed a simulation time of 1900 s and required a total of 96 h of CPU time. As anticipated, the adoption of such a simplified approach resulted in notable disparities with experimental data. The calculated transient temperatures at three selected locations have been compared with experimental data, Fig. 8. Experimental data indicates that the tank's bottom stagnant region experiences a rapid temperature increase until it disappears, leading to a two-phase flow regime (water and vapor mixture) throughout the entire tank. This phenomenon is thought to result from the local velocity increase caused by steam generation and the downward shift of the boiling front. However, simulations using the mixture model failed to replicate this abrupt temperature rise pattern, Fig. 8.

Overall, the mixture model approach was able to capture temperature transients during the initial stages of heat-up process, particularly when natural convection is the predominant heat transfer mechanism on

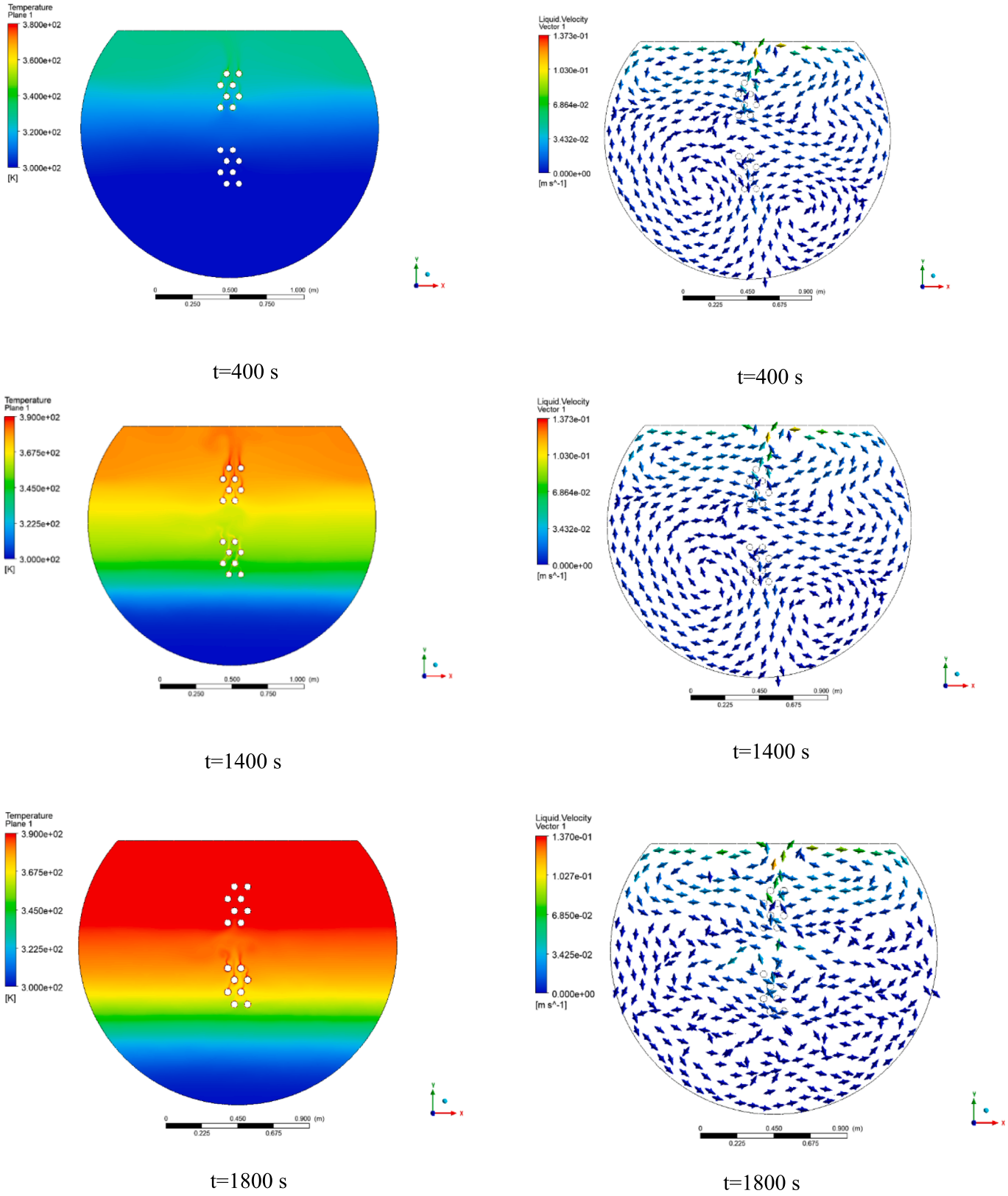

Fig. 7. Calculated temperature distribution and velocity contours with mixture model at different simulation times.

the secondary side. However, once boiling initiates, the model cannot predict sudden, local temperature increase. A comparable phenomenon was observed in the study conducted by Krepper et al. (Krepper and Beyer, 2010), wherein they employed single-phase CFD simulation to replicate natural circulation within the tank.

2D simulation with inhomogeneous Eulerian model

The temperature distribution and velocity contours in the secondary side calculated in simulations using Inhomogeneous Eulerian model in different simulation times are presented in Fig. 9. The sequential representation of temperature distribution over simulation time reveals a

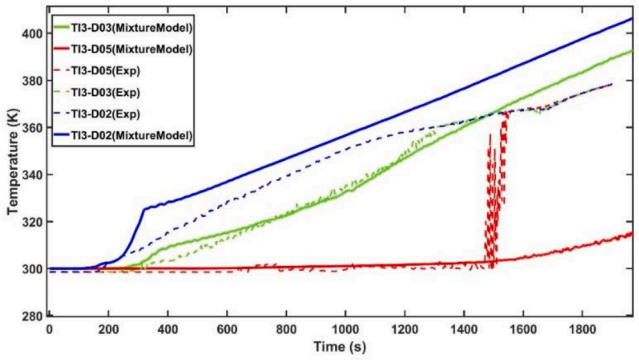

Fig. 8. Comparison of the transient temperatures from CFD simulations (single phase and mixture model) and experimental data.

notable disparity between the calculated temperature evolution during the heating-up process with inhomogeneous Eulerian model and the results obtained via the mixture model. In the Eulerian model outputs, although a stagnant zone is also observed at the bottom of the tank, it tends to dissipate gradually and faster after a certain duration from the start of the simulation. Initially, the temperature distribution exhibits greater resemblance to the mixture model in the earlier simulation times (e.g., t = 400). However, this pattern undergoes significant changes as the simulation time progresses.

The evolution of velocity contours also exhibits apparent variations. Initially, similar to mixture model, velocity gradients are primarily evident at higher elevations closer to the upper tube bundle. However, in Eulerian model, as the heating-up process continues, additional vortices emerge at the bottom of the tank due to heat transfer from the lower tube bundle. Moreover, as phase change phenomena commence after a certain duration, the velocity distribution in the bottom of the tank is further influenced. This phenomenon contributes to an abrupt increase in temperature in the lower regions of the tank.

The transient temperature of the same three locations as for the mixture model case have been compared with the experimental data as shown in Fig. 10. The Eulerian approach has led to considerable improvement of numerical results. Notably, the sudden temperature increase that has been observed in experiments in the lower region of the secondary side are effectively replicated. The CPU time required to execute these simulations utilizing an identical configuration on HPC cluster with unstructured mesh consisting of 123,707 elements amounted to 240 h. In this simulation, the average value of wall Y + for heated surfaces is 10 to calculate phase change phenomena using enhanced wall function properly. To evaluate the grid independence of the model, five distinct sets of computational grids are examined. The outcomes demonstrate the independency of the present mesh configuration in predicting temperature stratification and sudden temperature rise in the secondary side. Detailed information of mesh independence analysis can be found in supplementary materials.

4. Energy balance evaluation

To further validate the CFD methods, an energy balance evaluation has been carried out. The purpose of this assessment is to demonstrate the agreement between the computed total heat flux transferred to the fluid on the secondary side and the corresponding experimental data. The validation is based on the total heat flux when the steady state condition is reached in the process. This determination has been carried out through the utilization of Eq (2) in experimental data.

$$\dot{Q} = \dot{m}.C_p.\Delta T + \dot{m}.\Delta h_{phase} \quad (2)$$

Where ΔT it the temperature difference between inlet and outlet fluid of primary side, $\dot{m}$ is the mass flow rate and Δh_{phase} is latent heat of the fluid.

The transient heat flux transferred from tubes' wall to the adjacent fluid has been recorded in CFD codes for both Mixture and Eulerian model. The results of this calculation can be seen in Fig. 11. The transient nature of the heat up process can be seen in this figure.

The feasibility of calculating transient heat flux from experiments is hindered by the instrumentation utilized in NOKO facility. The temperature measurement in the primary loop was conducted only at the inlet and outlet. For the first 200 s of the experiment, the condensate does not reach the outlet, so the available temperature data is not representative of the actual temperature drop in the condensate and does not provide reliable means to calculate sensible heat transferred to the coolant. In addition, until all the initial cold water is removed from the primary loop, at least part of the heat of condensation and further cooldown is removed by mixing within the primary loop, rather than transported via tube wall to the pool. Therefore, a comparison was made between the calculated heat flux results from CFD and the steady-state heat flux observed in experiments. In practical terms, the heat flux transferring from the tube walls to the secondary side gradually increases throughout the process. This has been also represented in Fig. 11. It is noteworthy that the steady state condition is achieved earlier in experiments (as seen in Fig. 5) compared to CFD calculations due to the delay in sensing heat in the secondary side relative to the primary side. As it can be seen in Fig. 11, the deviation of calculated heat flux from CFD simulation and experiments in steady state condition is around ~12.5 %.

5. Conclusion

This research provides a detailed examination of various simulation techniques for accurately modelling temperature distribution, not only in the NOKO test facility but also broadly applicable to emergency condensers in nuclear power plants. While the NOKO facility served as a data source for validation, the methodologies and findings have wider implications. The study assesses different CFD simulations for predicting transient temperatures and proposes a new correlation that simplifies the calculation of heat transfer coefficients. This advancement reduces computational intensity and streamlines temperature analysis, benefiting various nuclear power plant contexts. The interdisciplinary approach enriches understanding of heat transfer and thermal dynamics in complex nuclear systems, emphasizing safety and optimization. These insights are valuable for the design and operation of nuclear reactors and have potential applications in enhancing CFD modelling across different engineering disciplines.

To summarize, the research surpasses its initial context of the NOKO facility, offering enhanced methods for predicting transient temperatures and calculating heat transfer coefficients in emergency condensers of nuclear power plants. It sets the stage for further investigations to advance safer and more efficient nuclear energy systems.

Nomenclature

A	area (m^2)
c_p	specific heat transfer [J $Kg^{-1}K^{-1}$]
D	diameter [m]
G	acceleration due to gravity [m s^{-2}]
Nu	Nusselt number
$\dot{m}$	mass flow rate [Kg/s]
P	pressure [pa]
Q	heat flux (W)
r	specific heat of vaporization [J kg^{-1}]
T	temperature [K] or [°C]
x	thickness [m]
λ	thermal conductivity [W m^{-1} K^{-1}]
Non-dimensional numbers	
Pr	Prandtl number
Abbreviations	
HTC	heat transfer coefficient [W m^{-2} K^{-1}]
St. St	stainless steel

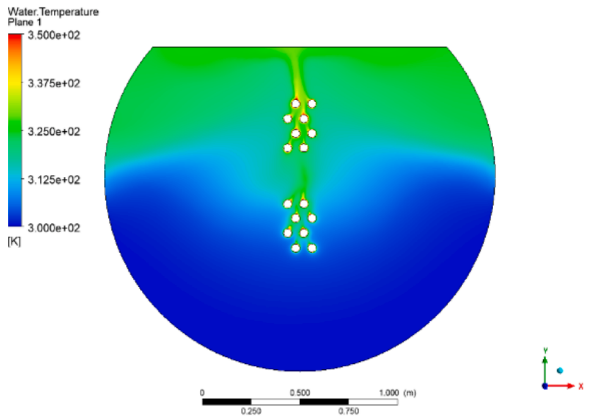

t=400 s

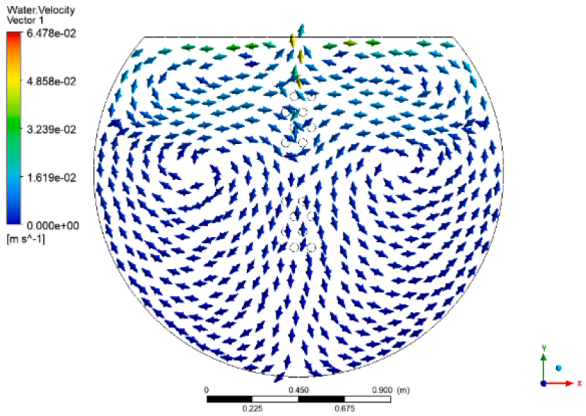

t=400 s

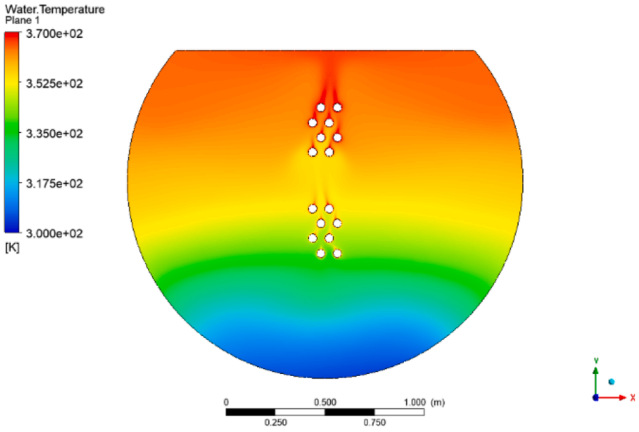

t=1400

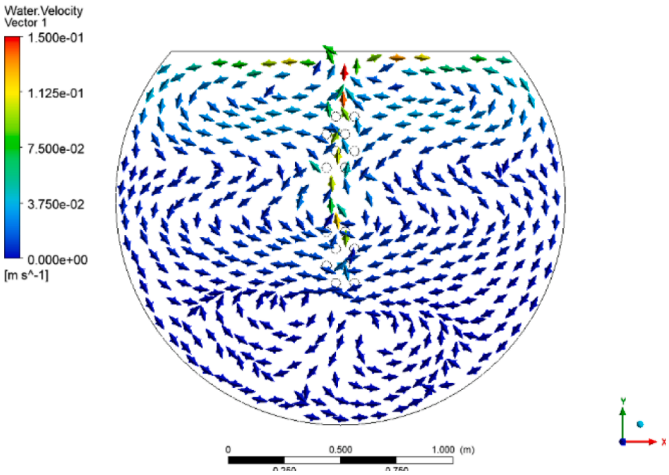

t=1400 s

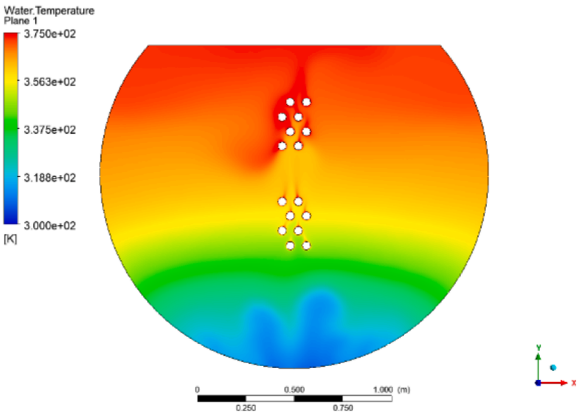

t=1800 s

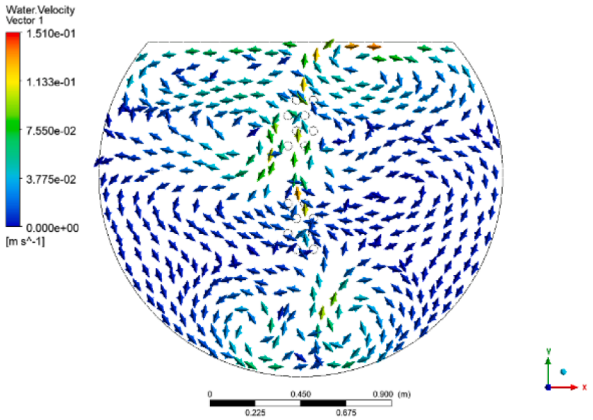

t=1800 s

Fig. 9. Temperature distribution and velocity contours calculated by Inhomogeneous Eulerian model at different simulation times.

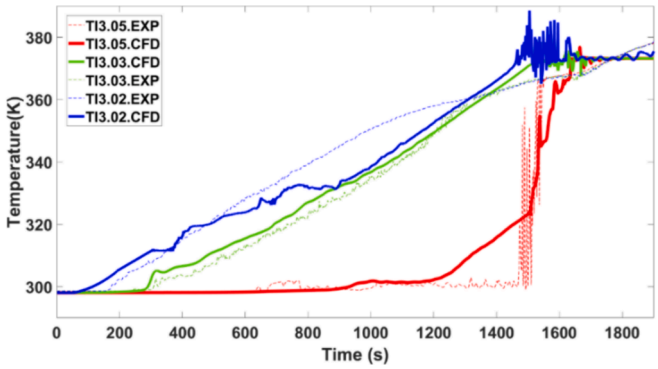

Fig. 10. Calculated and measured transient temperature, using Eulerian multiphase model.

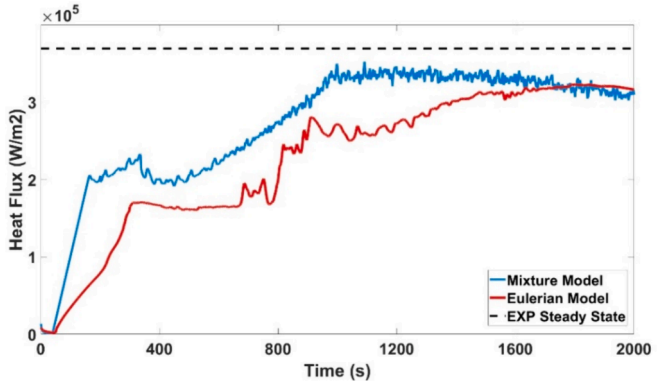

Fig. 11. Total heat transfer rate from primary side to the secondary side.

CRediT authorship contribution statement

Tahmineh Adili: Writing – review & editing, Writing – original draft, Visualization, Validation, Software, Methodology, Investigation, Formal analysis, Conceptualization. **Iurii Dolganov:** Methodology. **Filip Janasz:** Methodology, Investigation. **Stephan Leyer:** Supervision, Resources, Methodology.

Declaration of competing interest

The authors declare the following financial interests/personal relationships which may be considered as potential competing interests: The authors declare the following financial interests/personal relationships which may be considered as potential competing interests: Tahmineh Adili reports article publishing charges was provided by University of Luxembourg. If there are other authors, they declare that they have no known competing financial interests or personal relationships that could have appeared to influence the work reported in this paper.

Data availability

Data will be made available on request.

Appendix A. Supplementary data

Supplementary data to this article can be found online at https://doi.org/10.1016/j.nucengdes.2024.113260.

References

ANSYS, *ANSYS Theory Guide* 2022: ANSYS.
M.-H., Chun, Kang, M.-G., 1998. Effects of heat exchanger tube parameters on nucleate pool boiling heat transfer.
Cooper, M., 1984. Heat flow rates in saturated nucleate pool boiling-a wide-ranging examination using reduced properties. In: Advances in Heat Transfer. Elsevier, pp. 157–239.
Cornwell, K., Houston, S., 1994. Nucleate pool boiling on horizontal tubes: a convection-based correlation. Int. J. Heat Mass Transfer 37, 303–309.
Forster, H., Zuber, N., 1955. Dynamics of vapor bubbles and boiling heat transfer. AIChE J. 1 (4), 531–535.
Gorenflo, D., 1993. Pool Boiling, VDI Heat Atlas. VDI-Verlag, Dusseldorf, Germany.
Hibiki, T., Ishii, M., 2000. One-group interfacial area transport of bubbly flows in vertical round tubes. Int. J. Heat Mass Transfer 43 (15), 2711–2726.
Hicken, E.F., Verfondern, K., 2000. Investigation of the Effectiveness of Innovative Passive Safety Systems for Boiling Water Reactors. Forschungszentrum Jülich GmbH, Zentralbibliothek.
Hicken, E., et al., Pool heat-up experiments: experimental results from NOKO-EC tests. INNO-IPSS (99)-D-2.1, 2000. 9.
T. Hollands, H.A., C. Bals, S. Buchholz, S. Ceuca, H. Hristov, A. Langenfeld, P. Pandazis, S. Palazzo, J. Preuß, L. Tiborcz, S. Weber, Validierung von Rechenprogrammen zur Simulation des Reaktorkühlkreislaufs unter Störund Unfallbedingungen. 2016: GRS.
Krepper, E., Beyer, M., 2010. Experimental and numerical investigations of natural circulation phenomena in passive safety systems for decay heat removal in large pools. Nucl. Eng. Des. 240 (10), 3170–3177.
Krepper, E., Schaffrath, A., Aszódi, A., 2000. Numerical simulation of the emergency condenser of the SWR-1000. Nucl. Sci. Eng. 135 (3), 267–279.
Krepper, E., Končar, B., Egorov, Y., 2007. CFD modelling of subcooled boiling—concept, validation and application to fuel assembly design. Nucl. Eng. Design 237 (7), 716–731.
Kruzhilin, G., 1947. Free-convection transfer of heat from a horizontal plate and boiling liquid. Doklady AN SSSR (reports of the USSR Academy of Sciences) 58 (8), 1657–1660.
Kutateladze, S.S., V.M. Borishanskii, and A. d JB, A concise encyclopedia of heat transfer. 2021.
Labuntsov, D., 1973. Heat transfer problems with nucleate boiling of liquids. Therm. Eng. (USSR) (ENGL. Transl.) 19 (9), 21–28.
Lawrence, K., ANSYS Tutorial Release 2020. 2020: SDC Publications.
Rohsenow, W.M., 1952. A method of correlating heat-transfer data for surface boiling of liquids. Trans. Am. Soc. Mech. Eng. 74 (6), 969–975.
Sato, Y., Sekoguchi, K., 1979. Liquid Velocity Distribution in Two-Phase Bubbly Flow. Int. J. Multiphase Flow. 2 (79).
Schiller, L., 1933. A drag coefficient correlation. Zeit. Ver. Deutsch. Ing. 77, 318–320.
Shabestary, A.M., et al., 2020. Modelling of passive heat removal systems: a review with reference to the Framatome KERENA BWR reactor: Part I. Energies 13 (1), 35.
Stephan, K., Abdelsalam, M., 1980. Heat-transfer correlations for natural convection boiling. Int. J. Heat Mass Transfer 23 (1), 73–87.
Tian, Y., Zhang, K., Wang, N., Cui, Z., Cheng, L., 2017. Numerical study of pool boiling heat transfer in a large-scale confined space. Appl. Therm. Eng. 118, 188–198.
Tomiyama, A., et al., 1992. Numerical analyses of air lift pumps based on the multi-fluid model. Japanese J. Multiphase Flow 6 (2), 173–188.
Zhang, Y., et al., 2019. Evaluation of Stratified Condensation Models for a slightly inclined tube unsing ATHELT Code. NURETH-18.